Class. Quantum Grav. **25** (2008) 184002 (10pp) doi:10.1088/0264-9381/25/18/184002

The Schenberg data acquisition and analysis: results from its first commissioning run

César A Costa[1], Odylio D Aguiar[1], Nei F Oliveira Jr[2], Xavier Gratens[2], Sérgio T de Souza[2] and Sergio R Furtado[1]

[1] Divisão de Astrofísica, Instituto Nacional de Pesquisas Espaciais, São José dos Campos SP, Brazil
[2] Instituto de Física, Universidade de São Paulo, São Paulo SP, Brazil

E-mail: cesar@das.inpe.br

Received 31 March 2008, in final form 30 June 2008
Published 2 September 2008
Online at stacks.iop.org/CQG/25/184002

Abstract
The Mario Schenberg gravitational wave detector has started its commissioning phase at the Physics Institute of the University of Sao Paulo. We have collected almost 200 h of data from the instrument in order to check out its behavior and performance. We have also been developing a data acquisition system for it under a VXI System. Such a system is composed of an analog-to-digital converter and a GPS receiver for time synchronization. We have been building the software that controls and sets up the data acquisition. Here we present an overview of the Mario Schenberg detector and its data acquisition system, some results from the first commissioning run and solutions for some problems we have identified.

PACS numbers: 95.85.Sz, 04.80.Nn, 95.55.Ym

(Some figures in this article are in colour only in the electronic version)

1. Introduction

Gravitational waves (GWs) are an oscillatory solution for Einstein's field equations. They are local metric perturbations caused by accelerated masses. A passing GW can excite (quadrupolar) normal modes of elastic bodies, this concept was used by Joseph Weber at the end of the 1960s in order to demonstrate that their detection could be possible [1].

Robert Forward was the first to suggest a sphere as the antenna element in the early 1970s [2]. Ashby and Dreitlein studied the reception of GWs by an elastic self-gravitating spherical antenna and found a set of equations to treat such a problem [3]. Following up on this idea, Wagoner and Paik found the lowest eigenvalues for the monopole and quadrupole modes of a uniform elastic sphere and calculated its cross-section [4].

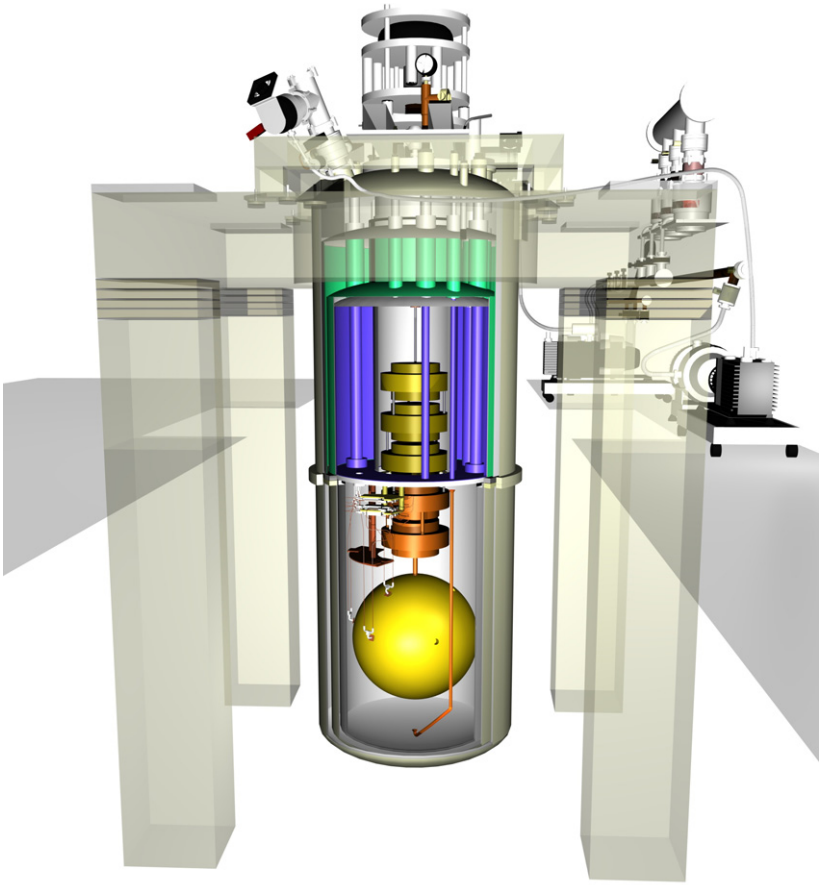

Figure 1. Schematic diagram of the Brazilian spherical Schenberg GW detector.

In the 1990s, Johnson and Merkowitz studied the antenna–transducer coupling problem and found an optimum configuration, which minimizes the number of transducers while keeping them in a symmetric distribution on the antenna: the truncated icosahedron (TI) configuration [5]. Magalhães and collaborators showed that distributions with more resonators can also have interesting symmetric properties [6, 7]. Lobo also suggested a more elaborated symmetric distribution [8].

Spherical gravitational wave detectors seem like an excellent low-cost alternative for GW detection. They have omnidirectional sensitivity and can give us some important information about an incident GW. A single spherical antenna can instantaneously determine the wave polarization and locate its astrophysical source in the sky for any GW signal detected. Moreover a sphere can be thought as five detectors in a single instrument [9]. The cross-correlation between normal modes reduces noise effects and increases detection possibility. Two of these instruments are being developed: the Brazilian Mario SCHENBERG [10] and the Dutch MiniGRAIL [11, 12].

Figure 1 shows a schematic view of the SCHENBERG detector. Its CuAl6% spherical element has 65 cm diameter and ∼1150 kg weight. The frequencies of the normal quadrupolar modes of such a sphere are $f_m \sim 3200$ Hz. The sphere is kept inside cryogenics chambers and

is suspended by a special developed suspension system. The spherical antenna is machined to have up to nine transducers. Such transducers should convert mechanical vibration into electric signals that could be later read for data analysis and GW signals searching.

Six of these machined positions follow the Johnson and Merkowitz's truncated icosahedron configuration (TI) [13]. Three other positions can be occupied by additional transducers which will be used for testing, calibrating, or monitoring other spherical modes.

We expect that when a standard quantum limit is reached, SCHENBERG will have a strain noise spectral density $\tilde{h} \sim 10^{-22}$ Hz$^{-1/2}$.

SCHENBERG had started its commissioning phase at the Physics Institute of the University of Sao Paulo. We tested the experimental parametric transducers and set up its data acquisition system. This work presents the instrumental configuration, its first data taking and the performance of the new data acquisition system.

2. The instrumental setup

Three experimental transducers were specially constructed for this initial phase. All of them are equipped with re-entrant klystron cavities [14]. Two transducers have one mechanical oscillatory mode which are tuned to be in a sphere quadrupolar frequency bandwidth ($\sim$3200 Hz). Such a mode works like a mechanical amplifier that increases the vibration amplitudes (about $\sim$150 times). The other one has no mechanical mode and therefore is directly coupled to the sphere vibration with no gain.

A microwave pump ($f_0 \sim 10.21$ GHz) [15] inserts a signal inline which is transmitted by microstrip antennas into the cavities. An intense electric field is developed across a variable short gap inside the cavity which modulates the inserted microwave signal [16]. The modulated signal returns throughout the microstrip antennas and is demodulated by a mixer device. The remaining signal carries information about the oscillation pattern inside the cavity [17]. Such information can be deconvolved by the instrumental transfer function and can allow the detection of a GW signal.

Figure 2(a) shows a schematic view of the non-resonant transducer. A detailed view of the microstrip pairs of antennas can be seen in figure 2(b). The transducers distribution is shown in figure 2(c).

Our tests indicated that these transducers show a low electrical quality factor ($Q_e \sim 10^4$) if no niobium layer is deposited on the internal walls of the cavity. The estimated $\mathrm{d}f/\mathrm{d}x$ was only $\sim$50 MHz mm^{-1}. These runs were performed during the third and fourth overall cryogenic cooldown in which the temperature of $\lesssim$5 K was reached.

We collected 120 h (five full days) of data from these three transducers with an analog-to-digital converter (ADC) IOTech-DaqBoard/2000 at sampling rate of 10 kHz. The data set was stored on a disk for further analysis.

During the analysis we noted many problems with spikes, gain fluctuations, dc level variations and voltage saturations in the output data for the first two commissioning runs. Such problems may be observed in figure 3. This figure presents a history of data taking where the root-mean-squared voltage of each 1 min file are plotted over time.

Strong voltage variations can be observed and they are caused by saturations and transients in the data. We have looked for possible causes of these voltage variations and have reached some assumptions.

We discovered that variations on the relative position of the microstrip antennas produce strong fluctuations on their signal reception. We measured this effect and the result is presented in figure 4(a). The saw teeth shape presented in figure 5 related to the relative distance was caused by the combination of a small compressed air leakage in the line and a hysteresis in the

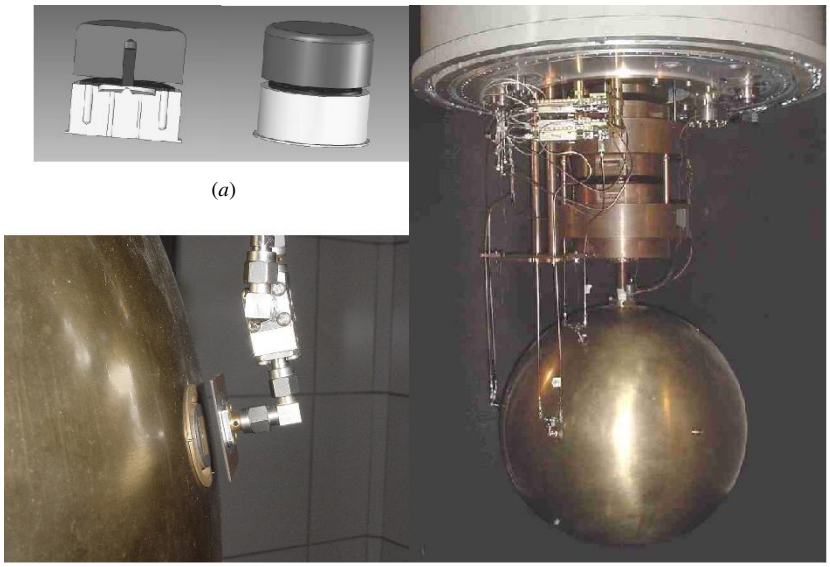

Figure 2. (*a*) Schematic view of the non-resonant transducer used in the first commissioning runs; (*b*) detailed view of the microstrip pair of antennas; (*c*) The position on the sphere surface of the three initial transducers can be seen.

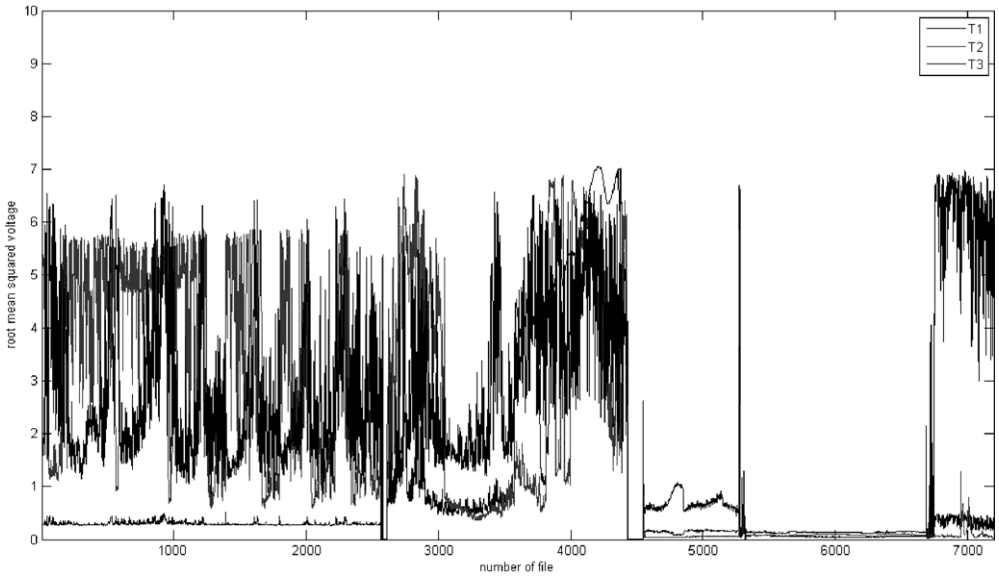

Figure 3. Root-mean-squared voltage (v_{rms}) for the 7200 1 min archives (120 h or five days of data). It represents a history of data acquisition. One can note gain variations along data taking.

valve that controls the pneumatic feedback action. Such hysteresis increased the differential pressure needed to activate the pressure regulator. This problem is now solved by changing such a valve for a more sensitive one with less hysteresis. Now the relative position changes $\lesssim$1 mm.

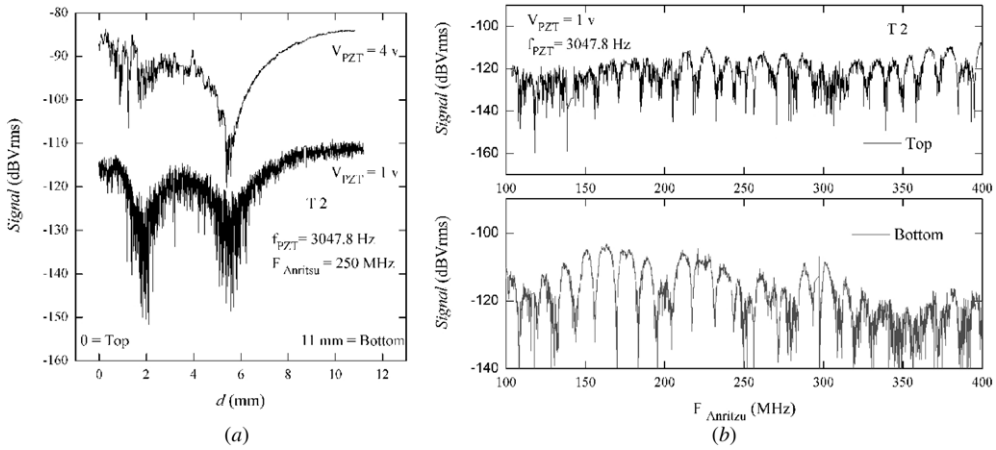

Figure 4. (*a*) Signal reception against the microstrip antennas relative distance. (*b*) Signal reception against the microwave pump frequency.

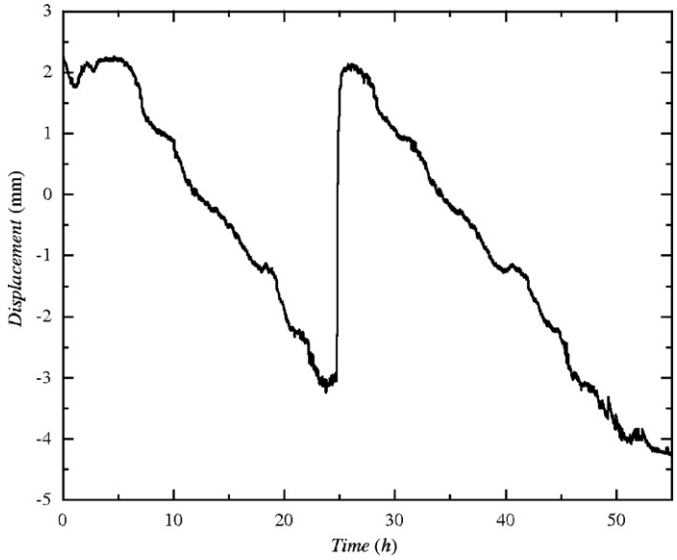

Figure 5. Variation of reception as a function of the distance of the microstrip antennas.

We also noted the presence of interferences along the demodulation process. Figure 4(*b*) shows how the reception changes when the microwave pump frequency sweeps some MHz. The first mode of the sphere (∼3046 Hz) was excited by a piezoelectric (PZT). The reception was measured while the microwave pump frequency was changed. During such a process we did not adjust the phase of the local oscillator signal. This action provides the maximum demodulation signal at the mixer output for an inserted frequency. Therefore we realized that such interferences were caused by different lengths of the transmission and the reception lines that generated this phase shift. We made some modifications in the transmission–reception lines and these interferences decreased.

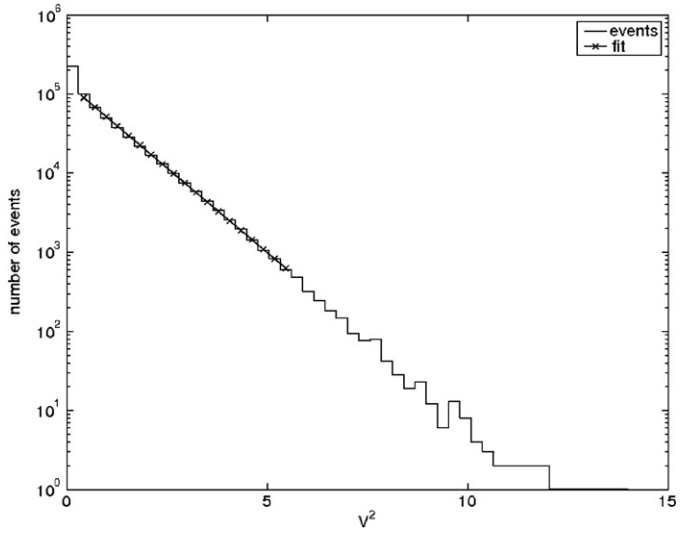

Figure 6. Histogram of the number of events as a function of voltage square.

But neither of these phenomena could explain the sudden gain variation observed, because both present long-period behaviors and can not be responsible for the spikes. After a long investigation by moving apart each piece along the line, we realized that some of the spikes were coming from a spectrum analyzer. It was connected in parallel to the reception line and some internal process during its self-calibration generates such spikes. It caused the dc level variations too. So now we know that it must be plugged off when data collection is triggered.

We now have a new data acquisition system (see section 4) and such problems no longer exist.

3. Some results from data analysis

Due to saturation problems we were able to find only about 12 hours (∼10% of the total time recorded) of useful data. From these data we generated histograms which show the number of events as a function of voltage squared. Once $V^2 \propto T$ figure 6 shows how it fits with a thermal distribution [18]

$$N = N_0 \exp -\frac{T}{T_0} \equiv N_0 \exp -\frac{V^2}{V_0^2}, \tag{1}$$

where N is the number of events in a bin, N_0 is the number of lowest energy events and $T_0 \propto V_0^2$ is the noise temperature.

The data were previously treated by a zero order prediction filter (ZOP) [19]. This fit and the lack of high energy events implies a Gaussian noise distribution, which is in agreement with a thermal distribution for this level of sensitivity (the fitted line in figure 6).

We have also estimated a scaled-strain noise, $K\tilde{h}$, in units of volts per meter per square root of hertz, where K is an unknown calibration constant. The quantity $K\tilde{h}$ is the product of the strain noise spectral density and the calibration constant K. This calibration constant tells us which voltage is obtained from the displacement inside the transducer resonant cavity ($\mathrm{d}V/\mathrm{d}x$). These first runs were performed with no calibration transducer and, so, we are not

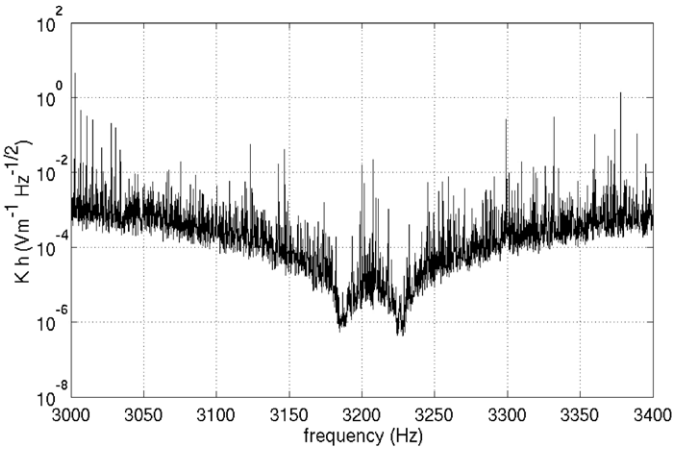

Figure 7. The scaled-strain amplitude spectral density. The calibration constant K was not measurable during these runs.

sure about the calibration parameters (such as eletro-mechanical coupling β_e, df/dx, etc). The scaled-strain amplitude spectral density is plotted in figure 7.

Such a curve has been obtained by a mathematical model of the mechanical transfer function [20–22]. The calculations of this transfer function take into account that we do not have all the six transducers of TI configuration. It implies that our pattern matrix has only two columns (from the two transducers on TI positions). We have considered the contributions of these two transducers to the normal modes and consequently to the spherical amplitudes h_m which are combined to obtain the strain noise

$$\tilde{h} = \sqrt{\sum_{m=1}^{5} h_m^2}. \tag{2}$$

Once we know the calibration constant K, the sensitivity curve can be obtained easily. The calibration transducer which has been constructed (and will be operational soon) will give us knowledge about the calibration constant K and about the sensitivity curve level in figure 7.

4. The new data acquisition system

The new Schenberg data acquisition system is now operational and ready for the next runs. It is based in a CT400 VXI Crater and is composed of:

Agilent E8491B is an IEEE-1394 PC link to VXI with a data transfer rate of ∼7 Mbytes/s through firewire;

VXI Technology VT1436 is a ADC with 24 bits precision, with 16 channels (simultaneous) acquiring up to 102 ksamples/s and anti-alias filtering;

Symmetricom BC357GPS is a GPS receiver with 10 MHz internal clock, 1 pps time referring and 16 bits time precision.

The data acquisition controller (DAC) software is running under Windows Server 2003, in a Dell Workstation (E8194 and VT1436 have no driver for Linux). All control software was written over C++ and works over the VXI platform using Agilent VISA Libraries.

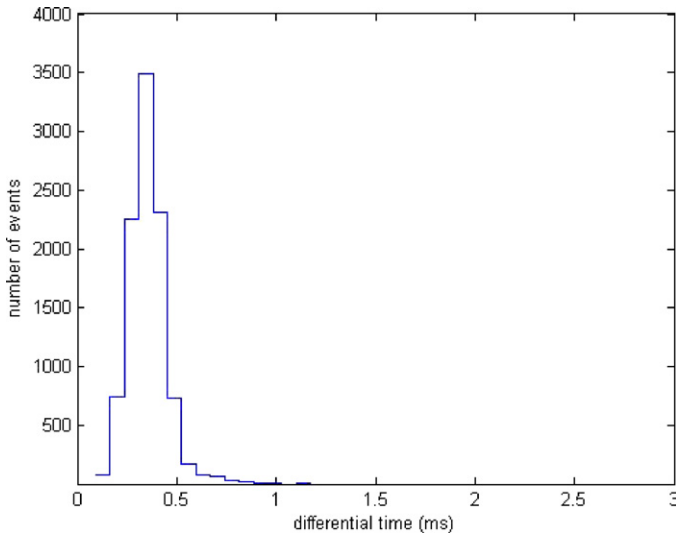

Figure 8. Histogram of requesting-receiving time interval which was estimated from 10 000 successively requested time stamps.

The DAC software sets up the GPS receiver and the VT1436 ADC triggers the data acquisition, takes time labels and stores data on a disk. Once data acquisition is triggered the VT1436 starts generating continuous blocks of data. When a block is ready an interruption becomes available. Such an interruption informs the GPS that a new block will start. The GPS acquires initial time stamps of data buffers produced by the ADCs and makes them available to the next agent in the acquisition chain.

All information is stored in a buffer like a sequential binary block. When a previously defined number of blocks are archived a file is opened, a header is written and such a block is recorded on a disk. The file header contains information about the number of blocks in the file, the number of sampled channels, the voltage range of samples, the sampling frequency, etc. So the data reader software can get such information for offline analysis.

We were interested in knowing if time registers are synchronized and timestamps truly correspond to the UTC time of data blocks.

4.1. Time synchronization

The main thread of the GPS agent spends most of its time waiting for new time stamps. When a time stamp is requested by the software it takes $\sim 3 \times 10^{-4}$ s to receive it and record it in a data buffer. Figure 8 shows a histogram of the delay on time register (estimated from 10 000 successively requested time stamps). Such a delay comes from the spent time between the DAC software's requesting, receiving, and recording time stamps. So the differential time associated with each data block (1024 samples at 25.6 kHz) was 0.32 ± 0.12 ms instead of 0.32 ms. This was very bad news since such a shift is larger than the time interval between several samples. And we could not know precisely the UTC time of each sample.

In order to circumvent such a problem we have introduced the 1 pps signal from the GPS receiver as an additional channel in the ADC. Once a new data file is opened a single time stamp is recorded in the header. It gives us the seconds of GPS time of the first 1 pps signal

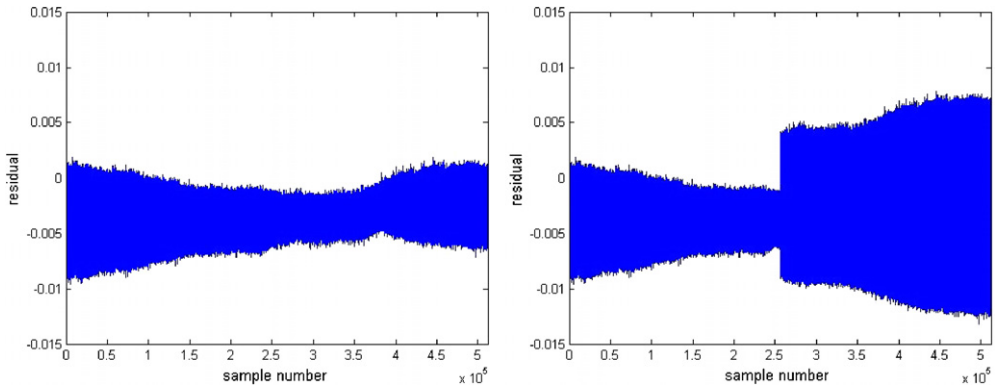

Figure 9. Residuals from collected data and modeled signal.

into it. So the GPS receiver no longer triggers the block acquisition, and it only gives us the UTC time of data samples.

We are now sure that we have a continuum data acquisition, so the blocks are sequential. We tested it by using known sine functions (sine wave from a function generator) which were inserted as a signal in the data acquisition system. We compared such acquired data with a perfect sine wave (mathematical model). Figure 9 shows residuals when collected data and modeled signal were compared. The figure on the left presents how real residuals are and that on the right presents how it must be if a delay of 1μs appears in sampled data.

Once no such thing can be observed in the data we are able to say that no sample was missed in this data set (over a day of continuum testing). No significant phase shift was observed so we have estimated that if it exists it may be $\delta\phi < 10^{-7}$.

5. Conclusions

We have made operational the data acquisition system for the Schenberg GW detector. Such a system proves to be efficient and matches the instrument requirements. Obviously, we are still working on the details, but this can be done without much effort taking into account the way the routines were written.

Much more work is still required to optimize this state-of-the-art instrument. This is the main goal of this stage: identification and troubleshooting instrumental problems. The results to date demonstrate a great potential for the instrument. The Mario Schenberg GW detector will soon be a great developed tool and can provide important information on astrophysical events that cannot be obtained otherwise.

Acknowledgments

CAC and ODA thank FAPESP (grant no. 05/00214-4, 98/13468-9 and 06/56041-3) and CNPq (grant no. 308759/06-0) for financial support.

References

[1] Weber J A 1960 *Phys. Rev.* **177** 306
[2] Forward R L 1971 *Gen. Rel. Grav.* **2** 149

[3] Ashby N and Dreitlein J 1975 *Phys. Rev.* D **12** 336
[4] Wagoner R V and Paik H J 1977 *Proc. Acad. Nazionale dei Lincei Intern. Symp. on Experim. Gravitation* (Singapore: World Scientific) p 257
[5] Johnson W W and Merkowitz S M 1993 *Phys. Rev. Lett.* **70** 2367
[6] Magalhães N S *et al* 1995 *Mon. Not. R. Astron. Soc.* **274** 670
[7] Magalhães N S *et al* 1997 *Gen. Rel. Grav.* **29** 1511
[8] Lobo J A 2000 *Mon. Not. R. Astron. Soc.* **316** 173
[9] Lenzi C H *et al* 2008 *Gen. Rel. Grav.* **40** 183
[10] Aguiar O *et al* 2006 *Class. Quantum Grav.* **23** S239
[11] De Waard A *et al* 2006 *Class. Quantum Grav.* **23** S79
[12] Gottardi L *et al* 2007 *Phys. Rev.* D **75** 102005
[13] Merkowitz S M and Johnson W W 1997 *Phys. Rev.* D **56** 7513
[14] Tobar M E *et al* 2000 *Gen. Rel. Grav.* **32** 1799
[15] Andrade L A *et al* 2004 *Class. Quantum Grav.* **21** S1215
[16] Barroso J J *et al* 2005 *Int. J. Infrared Millim. Waves* **26** 1071
[17] Aguiar O *et al* 2008 *Class. Quantum Grav.* **25** 114042
[18] Mauceli E *et al* 1997 *Phys. Rev.* D **56** 6081
[19] Heng I S *et al* 1999 *Class. Quantum Grav.* **16** 3439
[20] Costa C A and Aguiar O D 2006 *Preprint* gr/qc/0606112v1
[21] Merkowitz S 1998 *Phys. Rev.* D **58** 062002
[22] Gottardi L 2007 *Phys. Rev.* D **75** 022002